Solar Energy Materials & Solar Cells 149 (2016) 258–265

Contents lists available at ScienceDirect

Solar Energy Materials & Solar Cells

journal homepage: www.elsevier.com/locate/solmat

Improved evaluation of saturation currents and bulk lifetime in industrial Si solar cells by the quasi steady state photoconductance decay method

Binhui Liu [a], Yifeng Chen [b,*], Yang Yang [b], Daming Chen [b], Zhiqiang Feng [b], Pietro P. Altermatt [b], Pierre Verlinden [b], Hui Shen [a,c,d,*]

[a] Institute for Solar Energy Systems, School of Physics and Engineering, Sun Yat-Sen University, 5th Floor, C Block, Building of Engeneering, 132 Wai Huan Dong Road, Higher Education Mega Center, Guangzhou, Guangdong, PR China
[b] State Key Laboratory of PV Science and Technology, Trina Solar, No. 2 Trina Road, Trina PV Park, New District, Changzhou, Jiangsu, PR China
[c] Jiangsu Collaborative Innovation Center of Photovoltaic Science and Engineering, Changzhou University, No. 1 Gehu Road, Changzhou, Jiangsu Province, PR China
[d] Shun De SYSU Institute for Solar Energy, No. 1, Deshengdong Road, Shunde, Guangdong, PR China

ARTICLE INFO

Article history:
Received 9 December 2015
Received in revised form
24 January 2016
Accepted 26 January 2016
Available online 10 February 2016

Keywords:
Saturation current
QSSPC
Numerical simulation
Industrial solar cells

ABSTRACT

For understanding and improving the performance of industrial Si solar cells, it helps to quantify the losses in the various device parts very precisely, because this enhances the predictive power of roadmaps deduced from such analysis. We show how the precision of commonly applied methods for measuring the saturation current density, J_0, can be noticeably improved. Firstly, two methods are compared for determining the optical properties of the samples specifically made for lifetime measurements. Secondly, it is evaluated, which excess carrier density level is best to choose for extracting J_0 of the various device regions. Thirdly, the bulk lifetime is extracted by a combination of measurements and modeling of the surface passivation.

1. Introduction

For the improvement of the energy conversion efficiency of solar cells, it is crucial to know how the recombination losses are distributed among the emitter, base, and back-surface-field (BSF) region. This is so because reducing the recombination in the region with the highest recombination losses improves cell efficiency most effectively. The amount of recombination in the emitter and BSF regions is usually characterized by their saturation current density J_0. Commonly, J_0 is determined from measurements of the effective excess carrier lifetime, τ_{eff}, in dependence of the excess carrier density Δn, either via photo-conductance decay (PCD) applying the method of Kane and Swanson [1], or via quasi-steady-state photoconductance (QSSPC) as proposed by Sinton and Cuevas [2]. For samples with a high lifetime ($\tau_{\text{eff}} > 200\,\mu s$), the excess carrier decay is sufficiently slow so it can be monitored with PCD. For low lifetime samples, the flash duration is chosen to be longer than the excess carrier decay, so quasi-steady-state is reached where the rate of recombination, $\Delta n/\tau_{\text{eff}}$, is equal to the rate of generation G. Such methods have been successfully applied to the characterization of crystalline silicon and solar cells [3–8].

In this paper, we improve the precision of these methods, particularly for mass-produced, standard Si solar cells, which have a full-area BSF and a locally higher doped region at the front contacts (selective emitter). For example, the determination of G is critical. Assessment of G via a PC1D simulation is suggested [9]. However, for samples with a non-uniform surface like the Al-doped BSF, an accurate optical simulation is difficult [10]. Therefore, we stop the flash in the QSSPC measurement abruptly so it turns into a PCD measurement, and G is obtained by matching the resulting lifetime from both decays [11,12]. We compare this method with direct measurements of the reflectance and transmittance of our samples, which is introduced in SEMI PV13 [13]. Secondly, the extracted J_0 generally depends on Δn where it is extracted from τ_{eff}. We evaluate the proposal of Ref. [14] on choosing the optimum Δn for determining J_0. We extract the bulk lifetime by a combination of lifetime measurements and modeling.

2. The saturation current under illumination

The amount of recombination of excess carriers in device regions is commonly characterized by the saturation current

* Corresponding authors.
E-mail addresses: yifeng.chen01@trinasolar.com (Y. Chen), shenhui1956@163.com (H. Shen).

http://dx.doi.org/10.1016/j.solmat.2016.01.032
0927-0248/

density J_0. It is helpful to elucidate the reasons for this in order to obtain meaningful values for J_0 under illumination. The definition of J_0 originates from the diode in the dark. There, recombination enables the external current flow and, hence, the total recombination in the diode is equal to its external current. This basic fact makes it possible to determine the amount of recombination from the I–V curve. The original definition of J_0 comes from Shockley's ideal diode equation [15, p. 314], which links the external current density J with the external voltage V:

$$J(V) = J_0(e^{V/V_{\mathrm{th}}} - 1), \tag{1}$$

where J_0 is defined for the entire diode (not of a device region), V_{th} is the thermal voltage kT/q, with k being the Boltzmann's constant, T the absolute temperature, and q the elementary charge. Basically, J_0 is an equilibrium entity arising from the principle of detailed balance: it balances the drift current with the diffusion current in the device in thermal equilibrium (which is in the dark at zero applied bias). Nevertheless, J_0 is sometimes called 'reverse saturation current'. However, it bears ambiguities if J_0 is thought as originating from J at negative biases, because there no thermal equilibrium exists. The applied reverse bias merely forces the diffusion current toward zero so the drift current prevails with the size approximately equal to J_0, but in reality often deviates from J_0 obtained from the forward I–V curve. Therefore, it is only non-ambiguous to call J_0 the 'reverse saturation current' if it is indeed measured in the reverse bias range, which is rarely done.

As noted, J_0 as 'saturation current' has its well defined meaning in detailed balance, and this is so regardless whether an ideal diode model is applied (such as Shockley's) or more sophisticated models (e.g. beyond the drift-diffusion or depletion region approximation [16], or including photon recycling [17], and others). However, photovoltaic action does not occur in thermal equilibrium but under illumination. In order to still use the Shockley equation to relate J with V under illumination, it is common to simply subtract the short-circuit current density J_{sc} from Eq. (1):

$$J = J_0(e^{V/V_{th}} - 1) - J_{\mathrm{sc}}. \tag{2}$$

This approximation is commonly called the 'shifting approximation' or the superposition principle (because linearity in the semiconductor equations is assumed). It implies as if there were no recombination occurring at zero bias under illumination – while obviously the amount of $J_{\mathrm{rec}}(0) = |J_{\mathrm{gen}}| - |J_{\mathrm{sc}}|$ of the photogenerated current density J_{gen} is recombining. Therefore, it is important to be aware that J_0 can only be related to J and V under illumination if the amount of recombination due to the forward bias is significantly larger than the recombination due to illumination:

$$|J(V)| - |J_{\mathrm{sc}}| >> |J_{\mathrm{gen}}| - |J_{\mathrm{sc}}|. \tag{3}$$

Under 1-sun illumination, this condition is most often, but not always, fulfilled at the maximum power point (MPP) of the I–V curve of c-Si solar cells [18], but not of some other cell types [19].

Despite of these restrictions under illumination, the concept of J_0 is very useful for characterizing recombination in the various device parts of solar cells mainly because the concept can also be applied locally in the device: the external V lowers the built-in potential of the device, and a local voltage V_{loc} may be assigned to any position in the device. Because V_{loc} is equal to the separation of the quasi-Fermi energies, V_{loc} increases the product of the hole density p with the electron density n in an exponential manner according to the mass action law:

$$pn = n_{i,\mathrm{eff}}^2 e^{V_{\mathrm{loc}}/V_{\mathrm{th}}}. \tag{4}$$

where $n_{\mathrm{i,eff}}$ is the effective intrinsic carrier density, which is the intrinsic carrier density n_{i} affected by gap narrowing ΔE_{g}:

$$n_{\mathrm{i,eff}}^2 = n_{\mathrm{i}}^2 e^{\Delta E_{\mathrm{g}}/V_{\mathrm{th}}}. \tag{5}$$

Assigning Eq. (4) locally in Eq. (1) then yields:

$$J_{\mathrm{loc}} = J_{0,\mathrm{loc}}\left(\frac{pn}{n_{i,\mathrm{eff}}^2} - 1\right), \tag{6}$$

and after algebraic manipulation:

$$J_{0,\mathrm{loc}} = J_{\mathrm{loc}}\frac{n_{i,\mathrm{eff}}^2}{pn - n_{i,\mathrm{eff}}^2} \tag{7}$$

Generally speaking, $J_{0,\mathrm{loc}}$ is a measure for recombination in a device region because it is equal to the local current density J_{loc} that supplies the charge carriers for recombination in that device region, scaled by the quotient part of the formula where the excess carrier density Δn is involved, as is necessary when considering recombination rates of excess carriers. The term $pn - n_{\mathrm{i,eff}}^2$ is only equal to Δn in a quasi-neutral region (not in a space-charge region), therefore, p, n, $n_{\mathrm{i,eff}}^2$, and J_{loc} must be probed in the quasi-neutral region at the border of the local device region of interest. The 'loc' in $J_{0,\mathrm{loc}}$ of the emitter or BSF is commonly replaced by 'em', 'e', or BSF, or more generally by n^+ or p^+.

Please note that the derivation of Eq. (7) is very general, because it makes use of only two basic entities: the built-in potential, which is necessary for photovoltaic action [20], and the mass action law, which is valid for the magnitudes of the built-in voltage, regardless whether device parts are doped so highly that they are degenerated and Fermi-Dirac statistics needs to be applied. Because Eq. (7) is so general, it serves as a definition of $J_{0,\mathrm{loc}}$ in a similar manner as Eq. (1) serves as a definition of J_0: in thermal equilibrium, we again have a balance of currents obeying the principle of detailed balance. Therefore, it in unnecessary to name $J_{0,\mathrm{loc}}$ differently than the original J_0 (the name 'recombination pre-factor' was suggested in Ref. [21,22] but apparently has not been used in the PV community).

Unfortunately, the local p, n, and J_{loc} cannot be directly measured in the device, so Eq. (7) serves mainly for evaluating $J_{0,\mathrm{loc}}$ by means of simulations. However, $J_{0,\mathrm{loc}}$ can be indirectly extracted from measurements. For doing this, it has proven useful to prepare the sample such that the region of interest is confined near the surface of the sample. Then, the total recombination in the sample can be taken as the sum of bulk recombination and surface recombination, which is approximately:

$$\frac{1}{\tau_{\mathrm{eff}}} = \frac{1}{\tau_b} + \frac{2S_{\mathrm{eff}}}{W}, \tag{8}$$

where τ_{eff} is the measured lifetime ('effective' because it is usually influenced by various recombination mechanisms), τ_{b} is the bulk lifetime, W the thickness of the sample, and for two equal surfaces, a factor of 2 is inserted in front of S_{eff}. The effective surface recombination velocity S_{eff} is defined via its recombination current $J_{\mathrm{surf}} = q\ S_{\mathrm{eff}}\ \Delta n$, where Δn is assumed to be equal to the excess carrier density involved in τ_{eff} and τ_{b}. It is called 'effective' because surfaces are usually charged, so no quasi-neutrality exists. Hence, Δn must again be taken at a location where quasi-neutrality exists (e.g. in the quasi-neutral region of the sample just outside of the p–n junction or high–low junction). The last term of Eq. (8) is valid if S_{eff} is rather small [23], otherwise other expressions in Ref. [21] need be used. Because J_{surf} is a local current, we can now insert it in Eq. (6) and obtain:

$$S_{\mathrm{eff}} = \frac{J_{0,\mathrm{loc}}}{q\Delta n}\left(\frac{pn}{n_{i,\mathrm{eff}}^2} - 1\right). \tag{9}$$

With Eq. (9), Eq. (7) becomes [1]:

$$\frac{1}{\tau_{\text{eff}}}=\frac{1}{\tau_b}+J_{0,\text{loc}}\frac{\Delta n}{qn_{i,\text{eff}}^2 W}, \tag{10}$$

were we assumed that $pn/n_{i,\text{eff}}^2 \ll 1$. Hence, $J_{0,\text{loc}}$ is proportional to the steepness of the measured τ_{eff} curve if plotted as $1/\tau_{\text{eff}}$ over Δn, and is experimentally accessible via lifetime measurements as introduced in Ref. [1]. The method may also be applied if the base region is not in high-injection [24]. Two aspects are very useful when measuring $J_{0,\text{loc}}$ in this way:

1. For obtaining meaningful results for $J_{0,\text{loc}}$, it is important to be aware that small spatial variations in Δn in the device lead to measurement errors. This was addressed in Refs. [12,25] and will be dealt with in Section 5.2.

Note that the extracted $J_{0,\text{loc}}$ depends on $1/n_{i,\text{eff}}^2$, making it is necessary to state which value for $n_{i,\text{eff}}^2$ was chosen when publishing $J_{0,\text{loc}}$ results. Most commonly, either $n_{i,\text{eff}}=8.6\times10^9\ \text{cm}^{-3}$ (referring to 25 °C) or $n_{i,\text{eff}}=10^{10}\ \text{cm}^{-3}$ (at 300 K) are chosen. Other influences on the extracted $J_{0,\text{loc}}$ are discussed in Ref. [26]. During the lifetime measurement, V_{loc} fulfills the condition for V in Eq. (3) if the lifetime sample were contacted such that it acted as a solar cell. Hence, no other name than 'saturation current density' needs to be given to the measured $J_{0,\text{loc}}$, as was already stated in the discussion of its defining Eq. (7).

3. Determination of the carrier generation

3.1. Method with optical measurements

We use the lifetime tester WCT-120 from Sinton consulting, where Δn is monitored with a small solar cell next to the sample. Differences between the optical properties of the sample and the monitoring cell need be compensated for with the 'optical constant' F, i.e. there holds

$$\tau_{\text{QSS}}=\frac{\Delta n}{J_{\text{mc}}F} \tag{11}$$

where J_{mc} is the generation current given by the monitor cell. One way to determine F is to calculate the photogenerated current with the wavelength-dependent absorbance A and the photon flux $I_{\text{ph}}(\lambda)$ of the light pulse, and using

$$J_{\text{gen}}=q\int_{\lambda_{\min}}^{\lambda_{\max}} I_{\text{ph}}(\lambda)A(\lambda)\ d\lambda. \tag{12}$$

We obtain A via $A=1-T-R$ and measuring the reflectance R as well as the transmittance T with the sphere spectrophotometer Lunda 950. In the WCT-120 set-up, the optical constant is defined as unity when J_{gen} is 38 mA/cm^2, so the calculated F can be determined from:

$$F=\frac{J_{gen}}{38\ \text{mA/cm}^2} \tag{13}$$

Note that the parasitic absorption in the passivation and anti-reflection (ARC) layer is ignored, as well as via free carrier absorption (FCA), and can lead to an overestimation to J_{gen}. We placed the IR filter in front of the flash, which cuts off light with wavelengths above about 700 nm, so A of the passivation and ARC layer is small. However, the free carrier absorption does exist during the J_0 measurements of the emitter and the BSF, but the error is small and is neglected.

3.2. Method with transient lifetime measurements

As mentioned in the introduction, the flash can be abruptly stopped so the QSSPC measurement turns into a PCD measurement, and F is obtained by matching the resulting lifetime or J_0 from both decays:

$$F\approx\frac{J_{0,\text{trans}}}{J_{0,\text{QSS}}} \tag{14}$$

The approximations involved in this are elucidated in Ref. [11]. See also Refs. [12,13]. Fig. 1 shows a typical example where J_0 is measured with both the QSS and the transient method in dependence of Δn. $J_{0,\text{trans}}$ decreases drastically with increasing Δn (and will be explained in Section 5.2) while $J_{0,\text{QSS}}$ is rather unaffected for $\Delta n > 2\times10^{15}\ \text{cm}^{-3}$. By comparing $J_{0,\text{QSS}}$ with $J_{0,\text{trans}}$ at $\Delta n < 2\times10^{15}\ \text{cm}^{-3}$ we can acquire F.

3.3. Experiment

The two methods described above were employed to determine the optical constant of all sample structures, which are fabricated with 190 um p-type Cz wafers with a resistivity of near 20 Ω cm. Firstly, Fig. 2 shows $J_{0,\text{em}}$ as a function of Δn, measured with the transient method (filled symbols) and the QSS method (empty symbols). The optical constant is adjusted according to Eq. (14) such that the $J_{0,\text{em}}$ determined by QSS and by the transient

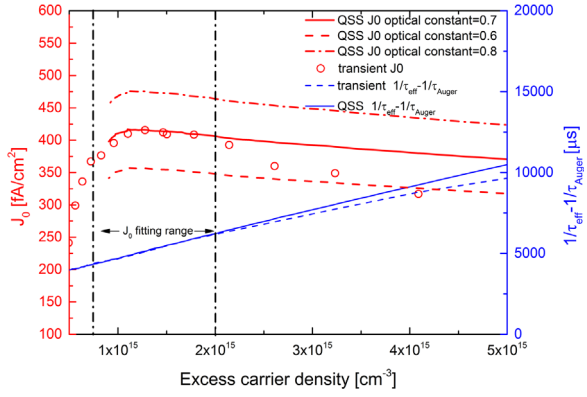

Fig. 1. An example of how lifetime measurements in either transient mode (blue dashed curve) or QSS mode (blue solid curve) influence the value of J_0 extracted by Eq. (10) (either open symbols or red lines). By tuning the optical constant, Eq. (14), J_0 in QSS mode scales as shown by the red dashed and red dot-dashed lines. (For interpretation of the references to color in this figure legend, the reader is referred to the web version of this article.)

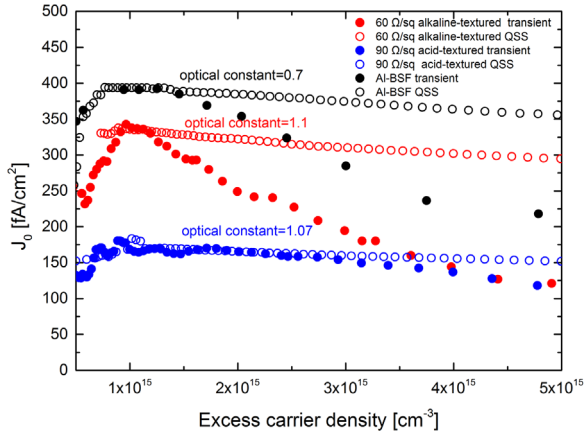

Fig. 2. Extraction of J0 from lifetime values measured either in QSS mode (empty symbols) or transient mode (filled symbols), and by adjusting the optical constants individually as indicated.

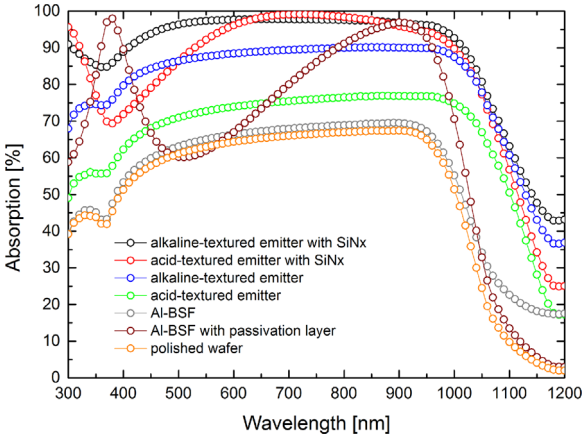

Fig. 3. Absorbance, measured with a sphere spectrophotometer, of the various types of silicon lifetime samples as a function of wavelengths.

Table 1
Optical constant of the emitter and BSF samples, determined either with the optical method using Eqs. (12) and (13) or by adjusting J_0 between QSS and transient method using Eq. (14).

Sample structure	Optical constant obtained with optical measurements	Optical constant obtained with comparing transient and QSS methods
Alkaline-textured emitter with SiN_x	1.11 ± 0.01	1.10 ± 0.02
Alkaline-textured emitter	1.00 ± 0.01	N/A
Acid-textured emitter with SiN_x	1.08 ± 0.01	1.07 ± 0.02
Acid-textured emitter	0.86 ± 0.01	N/A
Al-BSF	0.71 ± 0.01	0.70 ± 0.03
KOH etched Al-BSF	0.70 ± 0.02	0.70 ± 0.03
KOH etched Al-BSF with Al_2O_3/SiN_x	0.94 ± 0.02	0.95 ± 0.03
Polished wafer	0.68 ± 0.01	N/A

method agree: for emitter samples with 60 or 90 Ω/□, and the BSF samples, we obtain 1.1, 1.07 and 0.7, respectively. This shows that taking a single value from theoretical calculations may induce errors larger than 7%, which is commonly assumed as a lower bound [23,27] e.g. due to uncertainties in the determination of the sample thickness W in Eq. (10).

For illustrating the second method, Fig. 3 shows the measured absorbance, used to calculate the sample's photo-generation current using Eqs. (12) and (13). Table 1 lists the optical constants for different samples structures attained with the two different methods. Very good agreement is achieved. This shows that the parasitic absorption in the optical method does not significantly influence the extracted optical constant. Consequently, it is only necessary to use labor-intensive optical methods if the lifetime is too short for transient measurements.

4. Determination of the bulk lifetime

4.1. Methods

For analyzing the recombination losses in fabricated cells, it is necessary to determine their bulk lifetime τ_b at relevant Δn, which is near $10^{14}\,cm^{-3}$ at MPP and near $10^{15}\,cm^{-3}$ at open-circuit (the exact Δn depends on V_{mpp} and V_{oc}). In order to account for gettering and any contamination during cell fabrication, usually a finished cell is etched back on both sides, so only the

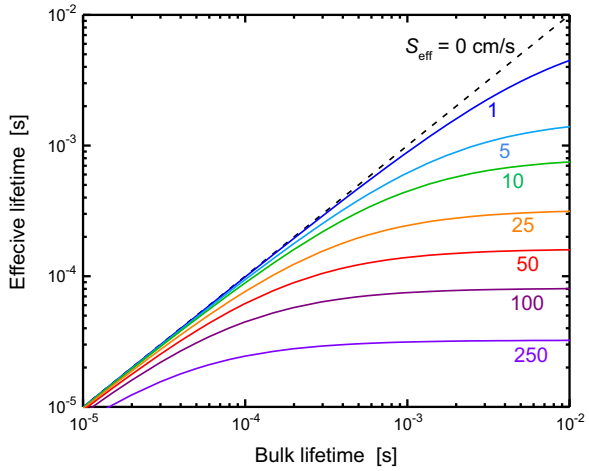

Fig. 4. The effective lifetime (that would be measured) of a 162 μm thick wafer as a function of its bulk lifetime for the indicated effective surface recombination velocities on both sides, calculated using Eq. (8).

base region survives. An alternative method is to remove a cell from fabrication just before metallization and etching off its emitter and BSF. Regardless which method is applied, the sample is subsequently passivated on both sides. With the first method, metal impurities that enter the cell via metallization are included in the analysis. This is not the case with the alternative method, but the sample stays pure and therefore cannot contaminate the cleaning bath and the passivation equipment.

Both surfaces need to be passivated so well that bulk recombination clearly dominates the total recombination at all relevant Δn or, if this cannot be assured, S_{eff} needs to be known or separately extracted. Fig. 4 shows τ_{eff} in dependence of τ_b for various S_{eff} of our c-Si wafer (162 μm thick), as calculated with Eq. (8). It is apparent that, above $\tau_b = 200$ μs, τ_{eff} is reduced by S_{eff} even for a Al_2O_3/SiN_x stack passivation, which yields approximately 10 cm/s [28,29]. Hence, surface recombination must be taken into account when extracting τ_b from the measured τ_{eff}. Note that a SiN_x passivation would yield higher S_{eff} values [30], which may even depend on injection density at low-injection if the wafer is damaged just below the surface by the SiN_x deposition [31,32] or if the sample is relatively small so edge effects become significant [30,33]. S_{eff} of oxidized samples is even higher and injection dependent even at low-injection due to the rather low fixed oxide charge [34].

There are a few experimental methods for determining τ_b as well as S_{eff} from τ_{eff} measurements. One method is to use corona charges to temporarily suppress surface recombination [35,36]; a laborious method is to vary the sample thickness W [37,38]; another method is to extract first S_{eff} by measuring τ_{eff} of a float-zone (FZ) sample (of similar resistivity and surface roughness as the etched-back cell) and assuming that surface recombination dominates [39]. We employ a method that combines experiment and numerical simulation, as explained in the following.

4.2. Experiment and simulation

We use p-type CZ c-Si as well as mc-Si wafers with resistivity near 2 Ω cm. The thickness of these two type wafers are both near 190 μm. After saw damage removal in a TMAH solution and RCA cleaning, the samples were diffused in a furnace with a $POCl_3$ standard diffusion step at 830 °C for 30 min. Then the PSG and the emitter were removed by THAH, followed by an Al_2O_3/SiN_x stack passivation [40–42] using plasma enhanced chemical vapor deposition (PECVD). In order to monitor the influence of diffusion and gettering on the bulk lifetime, reference wafers without

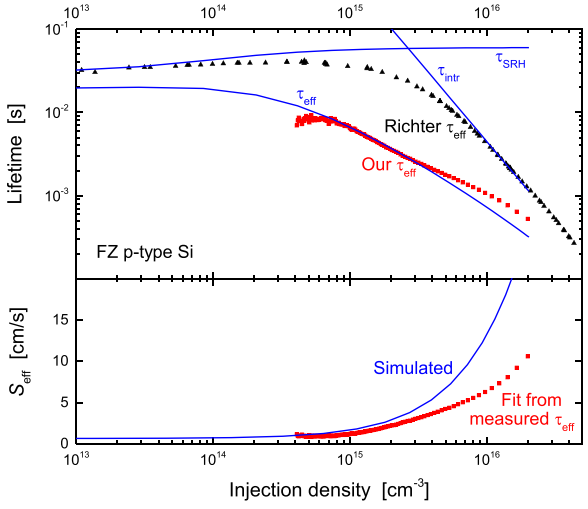

Fig. 5. The measured effective lifetime of a representative FZ wafer (symbols in top panel) is affected by surface recombation, and is compared to a measurement by Richter et al. [4] nearly unaffected by surface recombination. The effective surface recombination velocity (symbols in bottom panel) is extracted from the τ_{eff} measurement using Eq. (8), assuming the SRH and Auger lifetimes as indicated by the lines. The simulated S_{eff} (line in bottom panel) includes the model for Al_2O_3 from Ref. [42]. (For interpretation of the references to color in this figure, the reader is referred to the web version of this article.)

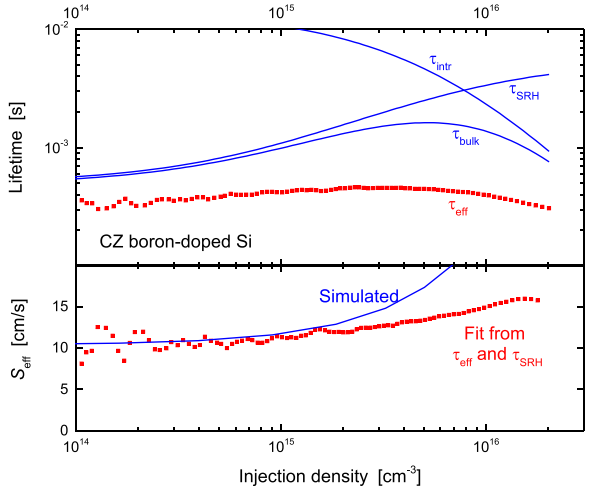

Fig. 6. The bulk lifetime (line in the upper panel) was extracted from the τ_{eff} measurement (symbols) by fitting the effective recombination velocity (symbols in bottom panel) to the simulated one (line) using Eq. (8), assuming the intrinsic carrier density of Ref. [4]. (For interpretation of the references to color in this figure legend, the reader is referred to the web version of this article.)

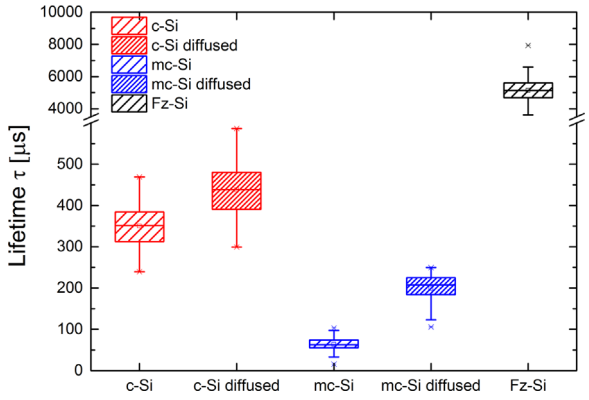

Fig. 7. Effective lifetimes, measured in the indicated samples at $\Delta n = 1 \times 10^{15}$ cm^{-3}, using the lifetime tester in the quasi-steady state mode.

diffusion were also prepared (with only saw damage removal and surface passivation). In order to extract the surface recombination velocity of the stack passivation, FZ wafers with a resistivity near 160 Ω cm were also used. Before the lifetime measurement, all the samples went through a standard firing step with 780 °C peak temperature for 2 s to activate the passivation layer.

Our basic strategy for extracting the bulk lifetime τ_b is to numerically simulate the surface passivation, first in a FZ wafer (for testing the model), then we include the surface model in the Cz wafer of interest to extract τ_b from Eq. (8). Fig. 5 shows our τ_{eff} measurement of the 160 Ω cm FZ wafer, and a simulation of it using the device simulator Sentaurus from Synopsys. Inputs to the simulations are the Si models of Ref. [43] with an update of the Auger recombination [4]. We take the model for Al_2O_3 passivation from Ref. [29], i.e. the cross-sections for electron and hole capture are $\sigma_n = 7 \times 10^{-15}$ cm^2 and $\sigma_p = 4 \times 10^{-16}$ cm^2. We take a single defect density of 2×10^{11} cm^{-2} and a fixed charge of -3×10^{12} cm^{-2} at the interface, both as measured in-house with the *C–V* technique on other samples not included in this paper; these values are compatible with literature of similar layers [44–48]. The only free parameters then are the Shockley-Read-Hall (SRH) lifetime parameters τ_n and τ_p. FZ material usually does not show a strong injection dependence of τ_{eff} when going from low to high-injection, so $\tau_p = \tau_n$ is a reasonable estimate. The simulations (blue lines in Fig. 5) fit the τ_{eff} measurements reasonably well with $\tau_p = \tau_n$ in the range between 20 ms and 50 ms. This range is reasonable, as shown in Fig. 5 by a comparison with data from Richter et al. [4] of a FZ wafer where surface recombination was very low (triangles). The difference between our τ_{eff} values and Richter's τ_{eff} values is attributed to surface recombination. Inserting our measured τ_{eff} values, the assumed τ_n and τ_p values, and the intrinsic lifetime [4] into Eq. (8) reveals the S_{eff} values shown as symbols, and coincides with the simulated S_{eff} values (blue line) at Δn below about 2×10^{15} cm^{-3}. To find agreement at higher Δn, we would need to choose the energy dependent defect densities and capture cross-sections [42,46]; we do not do this because the disagreement is outside of the Δn range relevant to solar cell operation at 1-sun illumination intensity.

Now we simulate our CZ samples, using exactly the same model for Al_2O_3 passivation as for the FZ wafer, see Fig. 6. In the CZ samples, the SRH lifetime is limited by the boron–oxygen complex, i.e. we choose $\tau_p = 10\tau_n$ [49–51], and in particular we set $\tau_n = 500$ μs to match the S_{eff} values (symbols), obtained from Eq. (8), with our simulated values (blue line). An $S_{eff} \approx 10$ cm/s is reasonable compared to literature values [26,27,29,43–46,52,53]. Please, note that τ_{bulk} is significantly higher than the measured τ_{eff} values. Thus, despite of using a high-quality Al_2O_3/SiN_x passivation stack, the evaluated τ_{bulk} and not the measured τ_{eff} values must be taken for assessing recombination losses in the cells, otherwise recombination in the base region is significantly over-estimated.

Fig. 7 shows the τ_{eff} values measured in about 70 wafers at $\Delta n = 1 \times 10^{15}$ cm^{-3}. A comparison with wafers that were not subjected to a phosphorus diffusion reveals that gettering improves τ_{bulk} by a factor of about 1.3 in case of CZ wafers, and of about 2 in case of mc-Si wafers.

5. Determination of J_0

5.1. Methods and sample preparation

For p-type commercial solar cells, the n^+ emitter is usually formed by $POCl_3$ diffusion in the furnace. Sometimes, a selective emitter (SE) [54] is formed, having a heavily diffused n^{++} region at the metal contacts to reduce the contact resistivity and

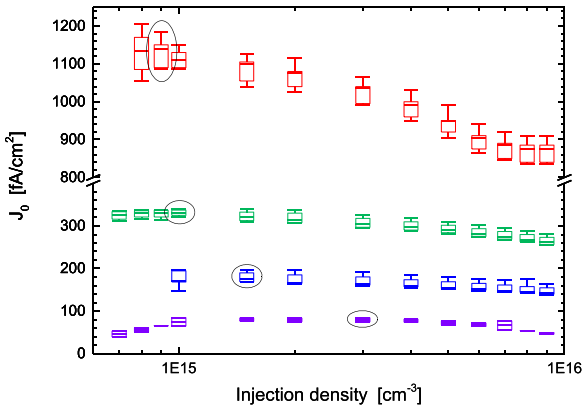

Fig. 8. Measured J_0 of the contacted part of the heavily diffused emitter (top), of its passivated part (next lower), of the passivated homogenous emitter, and of the passivated etched part (bottom). The circles indicate the maximum median value where J_0 is recommended to be taken [12], as listed in Table 2.

recombination at the contact [55], and a lightly-diffused n^+ part is formed between the contacts to reduce bulk recombination via inactive phosphorus [56] and for enabling effective surface passivation [57]. As the heavily-doped area is wider than the screen-printed Ag fingers for fulfilling the alignment tolerances in mass production, a separate measurement of the $J_{0,n+}$ (passivated), $J_{0,n++}$ (contacted) and $J_{0,n++}$ (passivated) is desirable. There are a few options to achieve this. One is to use the dynamic infrared lifetime mapping technique [58,59], which is not affected by metal, but needs to be carried out at elevated temperatures. A further method is to use common photoluminescence imaging [60–63], where the reflectivity of the metal needs be taken into account. Alternatively, the metallization fraction can be varied and $J_{0,n++}$ can be extracted by an open-circuit analysis [53]. Also lock-in thermography has been successfully used for determining J_0 with high spatial resolution [64]. We use the method where the metallization fraction is varied, but we remove the metal to perform a lifetime measurement, assuming that the surface recombination velocity is comparably high as with the metal [65]. Thus, we fabricated the following three types of samples.

Boron doped *p*-type CZ c-Si wafers with a resistivity near 20 Ω cm and with a thickness of 190 μm were used as substrates. These wafers were textured in TMAH solutions, featuring a random pyramid surface morphology on both sides. Then the diffusion step was carried out to form the selective emitter with a heavy diffusion of 60 Ω/□; the 150 Ω/□ lightly-doped part is formed in some of the samples by an extra etch-back process [66] with a HF/HNO_3 solution. SiN_x:H deposited by PECVD is employed for passivation of all samples and as an ARC.

The samples for the homogenous emitter (HE) were made in the same way, except that these wafers were textured in a HF/HNO_3 mixture solution, featuring typical acid-textured surface morphology, then diffused in the furnace to form a 90 Ω/□ emitter.

5.2. Measurements of the emitter J_0

Fig. 8 and Table 2 show J_0 extracted from QSS lifetime measurements of the various samples, using $n_i = 1 \times 10^{10}$ cm^{-3}. The optical constant for each sample was calibrated as shown in Table 1. According to Refs. [12,23], the variation of J_0 with Δn occurs because Δn at half-depth of the sample is higher than near the front and rear surfaces where the diffusions are located. Hence the average Δn, monitored by the lifetime tester, is higher than the Δn driving the amount of recombination in the diffused regions and, in turn, their J_0. This underestimates J_0, and therefore it is

Table 2
Emitter J_0 extracted as recommended by Ref. [12], indicated by the circles in Fig. 8, as well as at an injection level of 5×10^{15} cm^{-3} and 1×10^{16} cm^{-3}, as often done in literature.

Structure	ρ_{sh} [Ω/□]	J_0 @ maximum [fA/cm^2]	Δn @ maximum [cm^{-3}]	J_0 @ 10^{15} [fA/cm^2]	J_0 @ 10^{16} [fA/cm^2]
emitter (contacted)	60	1040 ± 44	9×10^{14}	950 ± 22	845 ± 33
emitter (passivated)	60	336 ± 20	1×10^{15}	294 ± 23	259 ± 20
emitter (passivated)	90	175 ± 18	2×10^{15}	154 ± 16	139 ± 15
emitter (passivated)	150	80 ± 7	3×10^{15}	72 ± 6	29 ± 2

recommended [12] to extract the J_0 value at the broad maximum (indicated by circles). It is apparent in Fig. 8 that this maximum occurs at higher Δn if the diffused region has a lower J_0. This is so because such regions draw less current for supplying their recombination, causing a smaller gradient of Δn in the base region towards the junction.

The box height in Fig. 8 is the usual interquartile range, while the whisker length from the median is chosen according to Tukey [67] as the nearest inner data point below twice the interquartile range. This enables us to discern outsiders. As uncertainties in Table 2 we use the box height times 0.7413 (which yields the standard deviation if the data distribution is Gaussian). These uncertainties turn out to be mostly near 7% precision, as expected from J_0 measurements [25]. Table 2 also lists the J_0 values extracted at $\Delta n = 5 \times 10^{15}$ cm^{-3} and 1×10^{16} cm^{-3}, as is often done in the literature. We will use them for an assessment in Section 6.

5.3. Al-alloyed sample preparation

The preparation and measurement of Al–B-alloyed BSF samples is slightly more involved, because only one side of the sample is alloyed in order to keep the firing conditions the same as in cell fabrication. We used the 20 Ω cm boron doped CZ Si wafer with a thickness of about 190 um as substrates as above. After saw damage removal and chemically polishing in the TMAH solution, the front surface was passivated with Al_2O_3/SiN_x:H, followed by screen-printing of an aluminum paste (containing boron) at the rear side. After firing in a belt conveyor furnace at 750 °C for alloying, the Al–Si eutectic layer and the Al residuals were removed in HCl solution. Additionally, some samples were etched in KOH solution for various times to obtain Al dopant profiles of different depth. The dopant profiles were measured with the electrochemical capacitance voltage (ECV) technique and applying the procedures in Ref. [68], using the Profiler CVP21 from WEP. In order to make a further study, some of these samples were additionally passivated with an Al_2O_3/SiN_x:H stack [69].

5.4. Measurement of J_0 of the Al–B-BSF

Fig. 9 shows J_0 of the samples, measured at Δn where J_0 is maximal, for various depth of the Al–B-BSF profiles. In the samples without surface passivation, recombination at the rear surface dominates. A thicker dopant profile constrains the minority carriers to reach the rear surface and to recombine there, so J_0 drops with increasing profile thickness. However, in the samples with surface passivation, bulk recombination dominates. Hence, J_0 increases with increasing profile thickness. The J_0 of the non-etched sample is

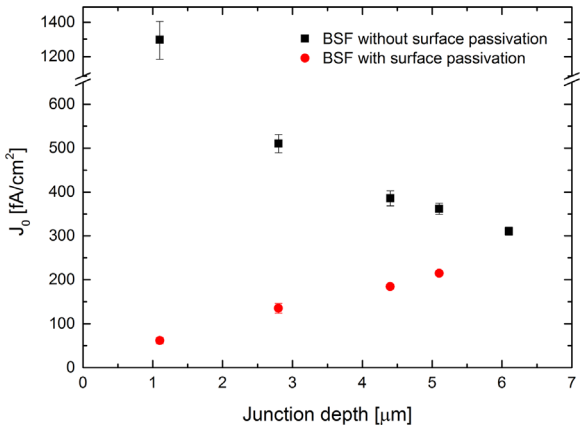

Fig. 9. The measured J_0 in the Al–B-alloyed region as a function of high–low junction depth for BSFs with (black squares) and without (red circles) surface passivation. (For interpretation of the references to color in this figure legend, the reader is referred to the web version of this article.)

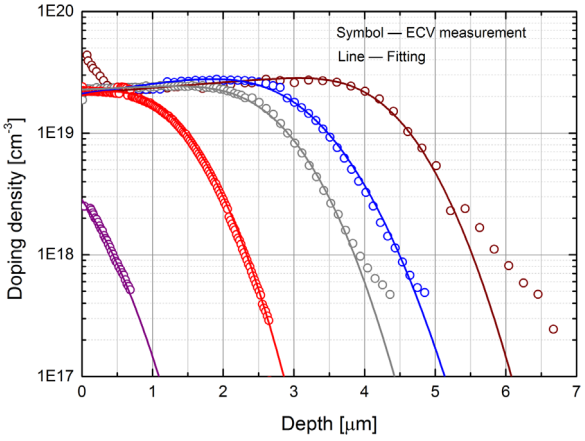

Fig. 10. The total dopant density (Al+B) of the Al–B-alloyed BSF, measured by the ECV technique (symbols) and fits (lines).

351 ± 7 fA/cm^2. This is similar as if no boron would have been added, but the density of the Al–O complexes would have been significantly reduced [70]. Indeed, boron increases the dopant density of the BSF by about a factor of 10 [71], see Fig. 10 for our dopant profiles measured with the same ECV set-up as described above. The ECV profiler measures the sum of Al and B, and is unaffected by the incomplete ionization of dopant atoms [72]. The higher dopant concentration reduces the minority carrier density and, with this, the SRH recombination rate via the Al–O defect levels.

6. Conclusion

For the further improvement of mass-fabricated crystalline silicon solar cells, it is beneficial to apply accurate characterization techniques that permit a loss analysis and, from there, a road map of equal precision. The saturation current J_0 needs to be evaluated at carefully chosen injection densities Δn, which depends on sample configurations. The bulk lifetime τ_b needs to be evaluated with taking account of surface recombination, despite the excellent passivation qualities of Al_2O_3 films. When using the lifetime tester in quasi-steady-state condition, a precise evaluation of the generation rate in the sample is important. It is shown that extracting J_0 from lifetime measurements at too high Δn may lead to significantly underestimated J_0 values.

Acknowledgments

This work is financially supported by the Science and Technology Planning Project of Guangdong Province (No. 2014B050505010) and the Natural Science Foundation of Jiangsu Province for Young Scientist (No. BK20140273).

References

[1] D.E. Kane, R.M. Swanson, Measurement of the emitter saturation current by a contactless photoconductivity decay method, in: Proceedings of the 18th IEEE Photovoltaic Specialists Conference, 1985, pp. 578–583.
[2] R.A. Sinton, A. Cuevas, Contactless determination of current–voltage characteristics and minority carrier lifetimes in semiconductors from quasi-steady-state photoconductance data, Appl. Phys. Lett. 69 (1996) 2510–2512.
[3] A. Cuevas, D. Macdonald, Measuring and interpreting the lifetime of silicon wafers, Sol. Energy 76 (2004) 255–262.
[4] A. Richter, S.W. Glunz, F. Werner, J. Schmidt, A. Cuevas, Improved quantitative description of Auger recombination in crystalline silicon, Phys. Rev. B 86 (2012) 165202.
[5] D.C. Walter, B. Lim, K. Bothe, R. Falster, V.V. Voronkov, J. Schmidt, Lifetimes exceeding 1 ms in 1-Ω cm boron-doped Cz-silicon, Sol. Energy Mater. Sol. Cells 131 (2014) 51–57.
[6] R. Woehl, P. Gundel, J. Krause, K. Rühle, F.D. Heinz, M. Rauer, C. Schmiga, M. C. Schubert, W. Warta, D. Biro, Evaluating the aluminum-alloyed p^+-layer of silicon solar cells by emitter saturation current density and optical microspectroscopy measurements, IEEE Trans. Electron. Dev. 58 (2011) 441–447.
[7] M. Rauer, C. Schmiga, M. Glatthaar, S.W. Glunz, Alloying from screen-printed aluminum pastes, containing boron additives, IEEE J. Photovolt. 3 (2013) 206–211.
[8] U. Römer, R. Peibst, T. Ohrdes, B. Lim, J. Krügener, E. Bugiel, T. Wietler, R. Brendel, Recombination behavior and contact resistance of n^+ and p^+ polycrystalline Si/mono-crystalline Si junctions, Sol. Energy Mater. Sol. Cells 131 (2014) 85–91.
[9] User manual of the WCT-120 photoconductance lifetime tester and optional Suns-Voc stage, Sinton Consulting, Boulder, CO, 2015.
[10] Z. Liu, N. Sahraei, B. Hoex, A.G. Aberle, I.M. Peters, Optical modeling of alkaline saw-damage-etched rear surfaces of monocrystalline silicon solar cells, IEEE J. PV 4 (2014) 1436–1444.
[11] T. Ohrdes, R. Peibst, N.P. Harder, P.P. Altermatt, R. Brendel, Characterization of the emitter collection efficiency by contactless photoconductance measurements, in: Proceedings of the 23rd Photovoltaic Science and Engineering Conference (PVSEC), Taipei, Taiwan, 2013, pp. 1216–1219.
[12] R. Lago-Aurrekoetxea, I. Tobías, C. Canizo, A. Luque, Lifetime measurements by photoconductance techniques in wafers immersed in a passivating liquid, J. Electrochem. Soc. 148 (2001) G200–G206.
[13] Test method for contactless excess-charge-carrier recombination lifetime measurement in silicon wafers, ingots, and bricks using an eddy-current sensor, SEMI PV13-0714 report, SEMI (Semiconductor equipment and Materials international, San Jose, CA), 2011.
[14] B. Min, A. Dastgheib-Shirazi, P.P. Altermatt, H. Kurz, Accurate determination of the emitter saturation current density for industrial P-diffused emitters, in: Proceedings of the 29th EU Photovoltaic Energy Conference, 2014, pp. 463–466.
[15] W. Shockley, Electrons and Holes in Semiconductors, 3rd edition, D. van Nostrand Company, New York, 1953.
[16] P.A. Markowich, C.A. Ringhofer, C. Schemiser, Semiconductor equations, Springer, NY, 1990.
[17] D. Lan, M.A. Green, Ideal solar cell equation in the presence of photon recycling, J. Appl. Phys. 116 (2014) 174511.
[18] S.J. Robinson, A.G. Aberle, M.A. Green, Departures from the principle of superposition in silicon solar cells, J. Appl. Phys. 76 (1994) 7920.
[19] A. Rothwarf, The superposition principle for current in solar cells, in: Proceedings of the 13th IEEE PV Specialists Conference, 1978, pp. 1312–1317.
[20] S.J. Fonash, Solar Cell Device Physics, second edition, Elsevier, New York (2010), p. 73.
[21] A. Cuevas, D. Yan, Misconceptions and misnomers in solar cells, IEEE J. of PV 3 (2013) 916–923.
[22] A. Thomson, N. Grant, K.F. Chern, T. Kho, Improved diffused-region recombination-current pre-factor analysis, Energy Procedia 55 (2014) 141–148.
[23] A.B. Sproul, Dimensionless solution of the equation describing the effect of surface recombination on carrier decay in semiconductors, J. Appl. Phys. 76 (1994) 2851–2854.
[24] C. Reichel, F. Granek, J. Benick, O. Schultz-Wittmanny, S.W. Glunz, Comparison of emitter saturation current densities determined by injection-dependent

lifetime spectroscopy in high and low injection regimes, Prog. PV 20 (2012) 21–30.
[25] H. Mäckel, K. Varner, On the determination of the emitter saturation current density from lifetime measurements of silicon devices, Prog. PV 21 (2013) 850–866.
[26] A.L. Blum, J.S. Swirhun, R.A. Sinton, A. Kimmerle, An updated analysis to the WCT-120 QSSPC measurement system using advanced device physics, In: Proceedings of the 28th EU Photovoltaic Energy Conference, 2013, pp. 1521–1523.
[27] A.F. Thomson, Z. Hameiri, N.E. Grant, C.J. Price, Y. Di, J. Spurgin, Uncertainty in photoconductance measurements of the emitter saturation current, IEEE J. PV 3 (2013) 1200–1207.
[28] L.E. Black, T. Allen, K.R. McIntosh, A. Cuevas, Effect of boron concentration on recombination at the p-Si–Al_2O_3 interface, J. Appl. Phys. 115 (2014) 093707.
[29] F. Werner, A. Cosceev, J. Schmidt, Interface recombination parameters of atomic-layer-deposited Al_2O_3 on crystalline silicon, J. Appl. Phys. 111 (2012) 073710.
[30] M.J. Kerr, A. Cuevas, Recombination at the interface between silicon and stoichiometric plasma silicon nitride, Semicond. Sci. Technol. 17 (2002) 166–172.
[31] S. Steingrube, P.P. Altermatt, D.S. Steingrube, J. Schmidt, R. Brendel, Interpretation of recombination at c-Si/SiN_x interfaces by surface damage, J. Appl. Phys. 108 (2010) 014506.
[32] Z. Hameiri, F.J. Ma, The impact of surface damage region and edge recombination on the effective lifetime of silicon wafers at low illumination conditions, J. Appl. Phys. 117 (2015) 085705.
[33] M. Kessler, T. Ohrdes, P.P. Altermatt, R. Brendel, The effect of sample edge recombination on the averaged injection-dependent carrier lifetime in silicon, J. Appl. Phys. 111 (2012) 054508.
[34] A.G. Aberle, Advanced Surface Passivation and Analysis, UNSW Press, Australia, 2001.
[35] M. Schöfthaler, R. Brendel, G. Langguth, J.H. Werner, High-quality surface passivation by corona-charged oxides for semiconductor surface characterization, In: Proceedings of the 1st World Conference on PV Energy Conversion, Waikaloa, HI, 1994, pp. 1509–1512.
[36] J. Schmidt, A.G. Aberle, Accurate method for the determination of bulk minority-carrier lifetimes of mono- and multicrystalline silicon wafers, J. Appl. Phys. 81 (1997) 6186–6199.
[37] E. Yablonovitch, D.L. Allara, C.C. Chang, T. Gmitter, T.B. Bright, Unusually low surface-recombination velocity on silicon and germanium surfaces, Phys. Rev. Lett. 57 (1986) 249–252.
[38] H. Kampwerth, S. Rein, S.W. Glunz, Pure experimental determination of surface recombination properties with high reliability, In: Proceedings of the 3rd World Conference on PV Energy Conversion, Osaka, Japan, 2003, pp. 1069–1107.
[39] M.J. Kerr, A. Cuevas, Very low bulk and surface recombination in oxidized silicon wafers, Semicond. Sci. Technol. 17 (2002) 35–38.
[40] J. Schmidt, B. Veith, R. Brendel, Effective surface passivation of crystalline silicon using ultrathin Al_2O_3 films and Al_2O_3/SiN_x stacks, Phys, Status Solidi RRL 3 (2009) 287–289.
[41] P. Saint-Cast, J. Benick, D. Kania, L. Weiss, M. Hofmann, J. Rentsch, R. Preu, S.W. Glunz, High-efficiency c-Si solar cells passivated with ALD and PECVD auminum oxide, IEEE Electron Device Lett. 31 (2010) 695–697.
[42] D.K. Simon, P.M. Jordan, I. Dirnstorfer, F. Benner, C. Richter, T. Mikolajick, Symmetrical Al_2O_3-based passivation layers for p- and n-type silicon, Solar Energy Mater. Solar Cells 131 (2014) 72–76.
[43] P.P. Altermatt, Models for numerical device simulations of crystallinesilicon solar cells – a review, J. Comput. Electron. 10 (2011) 314–331.
[44] L.E. Black, T. Allen, A. Cuevas, K.R. McIntosh, B. Veith, J. Schmidt, Thermal stability of silicon surface passivation by APCVD Al_2O_3, Solar Energy Mater. Solar Cells 120 (2014) 339–345.
[45] B. Liao, R. Stangl, F. Ma, T. Mueller, F. Lin, A.G. Aberle, C.S. Bhatia1, B. Hoex, Excellent c-Si surface passivation by thermal atomic layer deposited aluminum oxide after industrial firing activation, J. Phys. D: Appl. Phys. 46 (2013) 385102.
[46] M. Pawlik, J.P. Vilcot, M. Halbwax, M. Gauthier, N.L. Quang, Impact of the firing step on Al_2O_3 passivation on p-type Czochralski Si wafers: electrical and chemical approaches, Jpn. J. Appl. Phys. 54 (2015) 08KD21.
[47] D. Schuldis, A. Richter, J. Benick, P. Saint-Cast, M. Hermle, S.W. Glunz, Properties of the c-Si/Al_2O_3 interface of ultrathin atomic layer deposited Al_2O_3 layers capped by SiN_x for c-Si surface passivation, Appl. Phys. Lett. 105 (2014) 231601.
[48] L.E. Black, K.R. McIntosh, Modeling recombination at the Si–Al_2O_3 interface, IEEE J. PV 3 (2013) 936–943.
[49] K. Bothe, R. Sinton, J. Schmidt, Fundamental boron-oxygen-related carrier lifetime limit in mono- and multicrystalline silicon, Prog. PV 13 (2005) 287–296.
[50] J. Schmidt, A. Cuevas, Electronic properties of light-induced recombination centers in boron-doped Czochralski silicon, J. Appl. Phys 86 (1999) 3175–3180.
[51] S. Rein, S.W. Glunz, Electronic properties of the metastable defect in boron-doped Czochralski silicon: unambiguous determination by advanced lifetime spectroscopy, Appl. Phys. Lett. 82 (2003) 1054–1056.
[52] P. Saint-Cast, j Benick, d Kania, L. Weiss, M. Hofmann, J. Rentsch, R. Preu, S.W. Glunz, High-efficiency c-Si solar cells passivated with ALD and PECVD aluminum oxide, IEEE Electron. Device Lett. 31 (2010) 695–697.
[53] S. Bordihn, J.A. van Delft, M.M. Mandoc, J.W. Müller, W.M.M. Kessels, Surface passivation and simulated performance of solar cells with Al_2O_3/SiN_x rear dielectric stacks, IEEE J. PV 3 (2013) 970–9785.
[54] A. Neugroschel, F.A. Lindhom, S.C. Pao, J.G. Fossum, Emitter current suppression in a high-low-junction emitter solar cell using an oxide-charge-induced electron accumulation layer, Appl. Phys. Lett. 33 (1978) 168–170.
[55] T. Fellmeth, A. Born, A. Kimmerle, F. Clement, D. Biro, R. Preu, Recombination at metal-emitter interfaces of front contact technologies for highly efficient silicon solar cells, Energy Procedia 8 (2011) 115–121.
[56] B. Min, H. Wagner, A. Dastgheib-Shirazi, A. Kimmerle, H. Kurz, P.P. Altermatt, Heavily doped Si:P emitters of crystalline Si solar cells: recombination due to phosphorus precipitation, Phys. Status Solidi RRL 8 (2014) 680–684.
[57] P.P. Altermatt, J.O. Schumacher, A. Cuevas, M.J. Kerr, S.W. Glunz, R.R. King, G. Heiser, A. Schenk, Numerical modeling of highly doped Si:P emitters based of Fermi-Dirac statistics and self-consistent material parameters, J. Appl. Phys. 92 (2002) 3187–3197.
[58] J. Müller, K. Bothe, S. Gatz, H. Plagwitz, G. Schubert, R. Brendel, Contact formation and recombination at silicon solar cell base contacts, IEEE Trans. Electron Devices 58 (2011) 3239–3245.
[59] J. Müller, H. Hannebauer, C. Mader, F. Haase, K. Bothe, Dynamic infrared lifetime mapping for the measurement of the saturation current density of highly doped regions in silicon, IEEE J. PV 4 (2014) 540–548.
[60] M. Müller, P.P. Altermatt, K. Schlegel, G. Fischer, A method for imaging the emitter saturation current with lateral resolution, IEEE J. PV 2 (2012) 586–588.
[61] J. Müller, K. Bothe, S. Herlufsen, T. Ohrdes, R. Brendel, Reverse saturation current density imaging of highly doped regions in silicon employing photoluminescence measurements, IEEE J. PV 2 (2012) 473–478.
[62] X. Yang, D. Macdonald, A. Fell, A. Shalav, L. Xu, D. Walter, T. Ratcliff, E. Franklin, K. Weber, R. Elliman, Imaging of the relative saturation current density and sheet resistance of laser doped regions via photoluminescence, J. Appl. Phys. 114 (2013) 053107.
[63] W. Liang, K.J. Weber, D. Walter, T. Ratcliff, Emitter saturation current densities determined by selfconsistent calibration: impact of laterally non-uniform lifetime distribution on calibration accuracy, Energy Procedia 38 (2013) 114–123.
[64] S. Rißland, O. Breitenstein, High resolution saturation current density imaging at grain boundaries by lock-in thermography, Solar Energy Mater. Solar Cells 104 (2012) 121–124.
[65] V. Shanmugam, T. Mueller, A.G. Aberle, J. Wong, Determination of metal contact recombination parameters for silicon wafer solar cells by photoluminescence imaging, Solar Energy 118 (2015) 20–27.
[66] H. Haverkamp, A. Dastgheib-Shirazi, B. Raabe, F. Book, G. Hahn, Minimizing the electrical losses on the front side: development of a selective emitter process from a single diffusion, In: Proceedings of the 33rd IEEE Photovoltaic Specialists Conference, 2008.
[67] Robert McGill, John W. Tukey, Wayne A. Larsen, Variations of box plots, Am. Stat. 32 (1978) 12–16.
[68] R. Bock, P.P. Altermatt, J. Schmidt, Accurate extraction of doping profiles from electrochemical capacitance voltage measurements, In: Proceedings of the 23rd EU PV Solar Energy Conference, Valencia, Spain, 2008, pp. 1510–1513.
[69] R. Bock, J. Schmidt, R. Brendel, Effective passivation of highly aluminum-doped p-type silicon surfaces using amorphous silicon, Appl. Phys. Lett. 91 (2007) 112112.
[70] H. Steinkemper, M. Rauer, P.P. Altermatt, F.D. Heinz, C. Schmiga, M. Hermle, Adapted parameterization of incomplete ionization in aluminum-doped silicon and impact on numerical device simulation, J. Appl. Phys. 117 (2015) 074504.
[71] M. Rauer, C. Schmiga, M. Glatthaar, S.W. Glunz, Alloying from screen-printed aluminum pastes containing roron additives, IEEE J. PV 3 (2013) 206–211.
[72] M. Rauer, M. Rüdiger, C. Schmiga, H. Strutzberg, M. Bähr, M. Glatthaar, S.W. Glunz, Incomplete ionization of aluminum in silicon and its effect on accurate determination of doping profiles, J. Appl. Phys. 114 (2013) 203702.